Dissolution of Ionizable Drugs into Unbuffered Solution: A Comprehensive Model for Mass Transport and Reaction in the Rotating Disk Geometry

Marylee Z. Southard,[1,4] Don W. Green,[1] Valentino J. Stella,[2] and Kenneth J. Himmelstein[1,3]

Received July 10, 1990; accepted June 24, 1991

A model has been developed to describe the mass transport and reaction of ionizable compounds where mass transfer is caused by convection and diffusion from a rotating disk. Dissolution rates of benzoic acid, 2-naphthoic acid, and indomethacin in aqueous solutions of high ionic strength (I = 0.5 with potassium chloride) at 25°C were investigated. The model includes the effects of diffusion, convection, and simultaneous acid/base reaction at all points in the region adjacent to the dissolving solid. The solution of the transport equations is obtained numerically with an iterative algorithm which uses (a) closure of all material balances and (b) equilibria at the solid/liquid surface as constraints. The model solution yields both the flux of the dissolving acid and the concentration profile of each component. Reduced values of all reaction rate constants are used in the region adjacent to the dissolving surface to allow convergence of the computation. Although nonequilibrium concentration values are calculated, it is shown that the theoretical dissolution rate determined as the solution of the model is insensitive to the magnitude of the rate constants as their maximum useable values are approached. Comparisons of the model results with experimentally determined fluxes show close agreement and confirm that the transport mechanisms in the model formulation are consistent with the measured values. Further, the inclusion of convection allows accurate calculations without utilization of an arbitrary boundary layer thickness. Accurate dissolution rates can be determined using this technique under a wide range of conditions, except at low pH.

KEY WORDS: drug dissolution; rotating disk; mathematical model.

INTRODUCTION

The absorption rate of sparingly soluble drugs from the gastrointestinal tract can be limited by their dissolution rate, which is a function of hydrodynamics, medium characteristics, drug solubility, and other properties. Dissolution of such compounds in aqueous solution has been studied in the laboratory extensively over the past 50 years. Early studies (1–4) considered Fickian diffusion as the sole driving force to transport the dissolved compound from the solid surface to the bulk liquid. Film theory (5) was used in many diffusion models to define the stagnant region through which the dissolving drug moves. Because many drugs react in solution, the effects of chemical reaction also were incorporated into later work (6). Many recent efforts have used a rotating disk geometry since a constant film or boundary layer thickness has been shown to exist (7–16). Further, that film thickness can be estimated, as shown by Levich (17) for that system (18). Although the boundary layer defined by Levich was based on a physical system in which convection (due to bulk liquid flow generated by the disk rotation) and diffusion (due to a concentration gradient) are both important, workers modeling dissolution of reactive substances chose to omit the convective mechanism (7,15,16) or to confine all reactions occurring in the region to specific "planes" within which convection was omitted (11,14). In reality, transport of the dissolved drug from the solid tablet is affected by both mechanisms, while undergoing reversible acid–base reaction throughout the film. Thus, one or more components of the actual transport-reaction process were omitted from these models primarily because of computational difficulty (7).

An alternative approach to this problem is to obtain a numerical solution to the differential equations which describe the convection, diffusion, and reaction. The objective of this paper is to describe a numerical approach to formulate and solve a model for weak acid dissolution from a rotating disk into unbuffered aqueous solution (the buffered case will be considered in a separate study). The model includes the effects of convection and diffusion acting on the reactive components throughout the boundary layer. It incorporates the equilibrium reaction terms explicitly as forward and reverse reactions; thus this general approach is not limited to only reversibly or instantaneously reacting drugs. The model solution calculates the dissolution rate, or flux, of the dissolving acid and the concentrations of each reactive component at all points in the boundary layer.

The model presented here is specific for the rotating disk apparatus, which has been widely used to see relative changes in dissolution rates generated by a change in solution properties. Although fluid flows surrounding a dissolving tablet *in vivo* are much different from the rotating disk flow profile, the relative effects of solution pH can be accurately simulated by the present model. Further, the general modeling approach presented here can be applied to any dissolving weak acid where the fluid velocity is known at all points within a concentration boundary layer next to the solid surface.

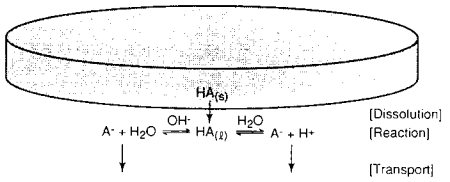

Fig. 1. Acid dissolution mechanism.

[1] Department of Chemical and Petroleum Engineering, 4006 Learned Hall, University of Kansas, Lawrence, Kansas 66045.
[2] Department of Pharmaceutical Chemistry, 3006 Malott Hall, University of Kansas, Lawrence, Kansas 66045.
[3] Department of Pharmaceutical Sciences, University of Nebraska Medical Center, Omaha, Nebraska 68198.
[4] To whom correspondence should be addressed.

0724-8741/92/0100-0058$06.50/0

MODEL DEVELOPMENT AND SOLUTION METHOD

The process of weak acid dissolution is shown in Fig. 1, where the acid (HA) dissolves in unbuffered aqueous solution. Following reversible reaction with water and hydroxide ion (OH^-) to produce the unprotonated acid (A^-), both acid species and H^+ can move away from the solid acid surface into the adjacent boundary layer. Thus there is a finite, nonzero flux of all transported species into the liquid layer due to instantaneous equilibrium reactions at the dissolving surface. Three reactions occur in aqueous solution:

$$HA \underset{k_{r1}}{\overset{k_{f1}}{\rightleftharpoons}} H^+ + A^- \tag{1}$$

$$H_2O \underset{k_{r2}}{\overset{k_{f2}}{\rightleftharpoons}} H^+ + OH^- \tag{2}$$

$$HA + H_2O \underset{k_{r3}}{\overset{k_{f3}}{\rightleftharpoons}} A^- + H_3O^+ \tag{3}$$

Because any two of the equations (1)–(3) can be combined to produce the third equation, only two of the three are linearly independent and completely define the equilibria. For the acid and water dissociation equations (1) and (2), equilibrium constants are (19)

$$K_a = \frac{k_{f1}}{k_{r1}} = \frac{[H^+][A^-]}{[HA]} \tag{4}$$

$$K_w = \frac{k_{f2}}{k_{r2}} = \frac{[H^+][OH^-]}{[H_2O]} \tag{5}$$

In a rotating disk apparatus, fluid flow adjacent to the tablet is generated as shown in Fig. 2. Fluid motion within a velocity boundary layer (δ_o) has velocity components in the x-, or axial direction; in the r-, or radial direction; and in the θ-, or angular direction. The distance h away from the tablet is the concentration boundary layer, the region through which acid concentration gradients are significant, and is much smaller than the velocity boundary layer, δ_o (17). The three velocity components, v_x, v_r, and v_θ, are functions of the axial distance from the tablet, x; the radial distance from the tablet center, r; and the angular velocity of the rotating disk, ω.

Transport Equations

For any dissolving compound, i, the differential equation describing transport in this configuration is (20)

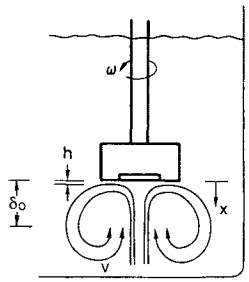

Fig. 2. Rotating disk apparatus.

$$\frac{\partial C_i}{\partial t} + v_r \frac{\partial C_i}{\partial r} + \frac{v_\theta}{r}\frac{\partial C_i}{\partial \theta} + v_x \frac{\partial C_i}{\partial x} = D_i\left[\frac{\partial^2 C_i}{\partial x^2} + \frac{\partial^2 C_i}{\partial r^2} + \frac{1}{r}\frac{\partial C_i}{\partial r} + \frac{1}{r^2}\frac{\partial^2 C_i}{\partial \theta^2}\right] + \phi_i \tag{6}$$

where C_i is the concentration of species i, and ϕ_i is the summation of the reaction terms appropriate for that compound. The terms on the right represent the change in flux of species i by diffusion. The second through fourth items represent convective transport due to the fluid motion. The time derivative $\partial C_i/\partial t$ represents the rate of change in concentration at any point within a distance h from the acid surface. It is assumed here that the diffusion coefficient (D_i) is neither concentration nor direction dependent. It is assumed also that there are no electrodiffusive effects caused by ionic species of different atomic or molecular weights.

An order-of-magnitude analysis has shown that the terms including radial and angular concentration gradients are insignificant compared to those in the axial direction (21). Thus the transport equations become

$$\frac{\partial C_i}{\partial t} = D_i \frac{\partial^2 C_i}{\partial x^2} - v_x \frac{\partial C_i}{\partial x} + \phi_i \tag{7}$$

Form of the Reaction Term

The forward and reverse reaction terms for each of the four components are incorporated into the differential equations (7) explicitly using the acid–base reactions (1) and (2), assuming elementary chemical reactions. The four mass balance equations to be solved for this system are

$$\frac{\partial C_{HA}}{\partial t} = D_{HA}\frac{\partial^2 C_{HA}}{\partial x^2} - v_x(x)\frac{\partial C_{HA}}{\partial x} + k_{r1}C_H C_A - k_{f1}C_{HA} \tag{8}$$

$$\frac{\partial C_A}{\partial t} = D_A\frac{\partial^2 C_A}{\partial x^2} - v_x(x)\frac{\partial C_A}{\partial x} + k_{f1}C_{HA} - k_{r1}C_H C_A \tag{9}$$

$$\frac{\partial C_H}{\partial t} = D_H\frac{\partial^2 C_H}{\partial x^2} - v_x(x)\frac{\partial C_H}{\partial x} + k_{f1}C_{HA} - k_{r1}C_H C_A + k_{f2}C_{H_2O} - k_{r2}C_H C_{OH} \tag{10}$$

$$\frac{\partial C_{OH}}{\partial t} = D_{OH}\frac{\partial^2 C_{OH}}{\partial x^2} - v_x(x)\frac{\partial C_{OH}}{\partial x} + k_{f2}C_{H_2O} - k_{r2}C_H C_{OH} \tag{11}$$

Boundary and Initial Conditions

To solve the transport equations above, boundary concentrations and initial conditions must be provided. Boundary conditions at all $t > 0$ are as follows.

$x = 0$	$x = \infty$
C_{HA} = acid solubility, C_S	$C_{HA} = 0$
C_A = unknown	$C_A = 0$
C_H = unknown	C_H = known from bulk solution pH
C_{OH} = unknown	C_{OH} = known from bulk solution pH

The outer boundary conditions are based on sink conditions for HA and A^- and bulk conditions for H^+ and

OH^-. For simplicity, rather than solving an "infinite" field, a finite boundary layer thickness is used in practice. The approximate thickness of this layer, h, has been determined by Levich as a function of a diffusivity D, the disk rotation rate ω, and the kinematic viscosity ν (17):

$$h = 1.61166\, D^{\frac{1}{3}} \nu^{\frac{1}{6}} \omega^{-\frac{1}{2}} \tag{12}$$

When this estimate is used in the present study, h is weighted through D for all four transported components, based on the contribution of each to the diffusive flux in the diffusion/reaction model (7) used to generate the initial condition. Details of the weighting method are given in Ref. 16. To approach the boundary condition at $x = \infty$, a concentration boundary layer several multiples of h in thickness is used.

Because the three unknown wall concentrations are to be related through the equilibrium equations (4) and (5), only one of the three unknown values is required independently to determine all three. The remaining boundary condition is determined assuming no flow of charge; that is, the sum of fluxes of all positively charged species equals the sum of all negatively charged species fluxes (7,16):

$$-D_H \left.\frac{dC_H}{dx}\right|_{x=0} = -D_A \left.\frac{dC_A}{dx}\right|_{x=0} - D_{OH} \left.\frac{dC_{OH}}{dx}\right|_{x=0} \tag{13}$$

There is no convective contribution in (13) because the axial and radial velocities are zero at the tablet wall.

The desired solution from this model is a simulation of concentration profiles within the boundary layer and a calculation of the steady-state flux of acid. To maintain stability in computation, the solution is obtained by progressing in measured time steps. Arrival at the steady-state condition is evident when the concentration profiles cease changing between time steps. Initial conditions are set to give an initial concentration profile for each component which is of similar shape to the expected solution profiles from this problem. Earlier researchers obtained an exact analytical solution to this problem without the convective term (7). In practice, any reasonable initial condition can be used since only steady-state simulation results are desired.

Model Parameters

The experimental conditions to be simulated (disk rotation rate, pH of the bulk aqueous solution surrounding the disk, and diffusivities of the dissociated species) and the chemical properties of the dissolving compound (solubility, diffusion coefficient, and dissociation constant) must be provided. The appropriate constants for the three weak acids considered in this study are shown in Table I.

Calculation of Acid Dissolution Rate

The desired result from the numerical model solution is the dissolution rate or flux of a specific acid. Because of the flow pattern generated by the disk rotation (Fig. 2), the flux of acid from a cylindrical control volume has both axial and radial components as shown in Fig. 3. A mass balance across the surfaces that define the control volume includes both a diffusive term due to the significant concentration gradient in the x-direction and a convective term generated from v_x and v_r. Because mass transport due to diffusion is a function of the position-dependent concentration gradient

$$J = -D \frac{dC}{dx} \tag{14}$$

and $\partial C/\partial r$ is small compared to $\partial C/\partial x$, there is no radial diffusion (17). However, flux due to bulk flow is a function of velocity and concentration. Since $v_r C_i$ is large at the edge of the disk, radial convection is significant. Thus, convective transport cannot be neglected in either the radial or the axial dimension. Angular transport has no effect on flux because v_θ does not move fluid across the system boundaries.

An acid mass rate balance around the control volume shown in Fig. 3 is

$$\text{accumulation rate} = \text{flux in} - \text{flux out} + \text{generation rate} \tag{15}$$

where flux represents the mass rate of all acid species (HA, A^-). Because no new acidic species are created once HA is in the boundary layer, the generation term in (15) is zero. At

Table I. Intrinsic Solubilities, Diffusion Coefficients, and K_a Values for Benzoic Acid, β-Naphthoic Acid, and Indomethacin at 25°C, and an Ionic Strength of 0.5 with Potassium Chloride (7,21)

Compound	Intrinsic solubility (M)	Diffusivity (cm^2/sec)	K_a	pK_a
Benzoic acid[a]	2.15×10^{-2}	9.7×10^{-6}	9.25×10^{-5}	4.03
β-Naphthoic acid	1.30×10^{-4}	6.1×10^{-6}	9.64×10^{-5}	4.02
Indomethacin	3.25×10^{-6}	5.6×10^{-6}	6.70×10^{-5}	4.17

[a] The diffusion coefficient of benzoate anion was determined as described in Ref. 21. Good agreement is seen with the benzoic acid diffusion coefficient calculated by Mooney *et al.* (7) as 9.6×10^{-6} cm^2/sec.

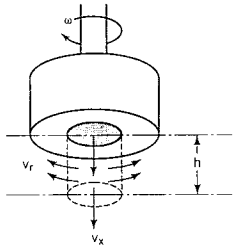

Fig. 3. Acid transport through a boundary layer near the rotating disk.

steady-state there is no accumulation. The flux balance from (15), including diffusive and convective terms, is

$$0 = \sum_{\substack{i \\ \text{acid} \\ \text{forms}}} (\pi R^2)\left(-D_i \frac{dC_i}{dx}\right)\Delta t\Big|_x + (\pi R^2) v_x C_i \Delta t|_x - (\pi R^2)\left(-D_i \frac{dC_i}{dx}\right)\Delta t\Big|_{x+\Delta x} - (\pi R^2) v_x C_i \Delta t|_{x+\Delta x} - (2\pi R) v_R(x) C_i \Delta x \Delta t \quad (16)$$

Dividing by $\pi R^2 \Delta t$, taking limits as $\Delta x \to 0$, and integrating (16),

$$0 = \sum_{\text{acid}}^{i} \int_0^h \frac{2}{R} v_R(x) C_i dx + \left[v_x C_i + -D_i \frac{dC_i}{dx} \right]\Bigg|_0^h \quad (17)$$

The final term in Eq. (17) is eliminated because $v_x = 0$ at $x = 0$, and the sink boundary condition imposed at $x = h$ states that $C_{HA} = C_A = 0$. The mass rate balance for acid transport is then

$$0 = \sum_{\text{acid}}^{i} \int_0^h \frac{2}{R} v_R(x) C_i(x) dx - D_i \frac{dC_i}{dx}\Bigg|_0^h \quad (18)$$

Thus, acid species enter and exit through the surfaces of the control volume parallel to the disk by diffusion and exit radially from the control surface normal to the disk by convection.

The integral in (18) can be evaluated using $v_R(x)$ for the rotating disk (17)

$$v_R(x) = aRx - bRx^2 + \cdots \quad (19)$$

where

$$a = 0.51023 \sqrt{\frac{\omega^3}{\nu}}, \qquad b = \frac{\omega^2}{\nu}$$

The mass rate balance around the control volume at steady state is

$$J_{\text{acid}} \text{ in} = J_{\text{acid}} \text{ out} \quad (20)$$

which, incorporating Eqs. (18) and (19), is

$$D_{HA}\left[-\frac{dC_{HA}}{dx}\Big|_{x=0} + -\frac{dC_A}{dx}\Big|_{x=0} \right] = D_{HA}\left[-\frac{dC_{HA}}{dx}\Big|_{x=h} + -\frac{dC_A}{dx}\Big|_{x=h} \right] + 2\int_0^h ax(C_{HA} + C_A) dx \quad (21)$$

The flux equation (21) contains the implicit assumption that $D_{HA} = D_A$, which has been shown experimentally to be accurate to 1% for benzoic acid and benzoate over a range of pH 4–9 (21). This same assumption was used without verification for the other acids studied. Once a solution to the transport equations (7) is determined, the acid species concentrations are known at all points across the control volume, and the integral and derivatives in Eq. (21) can be evaluated numerically. Therefore, the acid dissolution rate for a given acid and experimental condition is calculated directly from the solution of the fundamental transport equations.

Numerical Solution Method

Although steady state (constant dissolution rate) is reached rather quickly in the physical dissolution apparatus, use of an unsteady-state (time-dependent) formulation is essential to achieve a numerical solution of the equations above. The component concentrations vary with time as well as with distance from the rotating disk, approaching the desired steady-state condition in small time steps. A finite difference approximation of the derivatives in the four transport equations (7) was used to formulate a numerical representation for solution (22). To approximate Eqs. (7) in finite difference form, the concentration boundary layer is defined and divided into the desired number of divisions, N. Figure 4 illustrates this notation for $N = 4$, where Δx is the distance between each pair of adjacent space points. Thus, $\Delta x = h/N$, point $N + 1$ is the outer boundary point, and point 1 the wall point. Forward differences were used for the first derivatives, and a centered difference was used for the second derivative. The finite difference form of the HA transport equation is then

$$\frac{C_{i,j+1}^{(HA)} - C_{i,j}^{(HA)}}{\Delta t} = \frac{D_i}{(\Delta x)^2}\{C_{i-1,j+1}^{(HA)} - 2C_{i,j+1}^{(HA)} + C_{i+1,j+1}^{(HA)}\} - \frac{v_x}{\Delta x}\{C_{i+1,j+1}^{(HA)} - C_{i,j+1}^{(HA)}\} + k_{r1} C_{i,j}^{(A)} C_{i,j}^{(H)} - k_{f1} C_{i,j}^{(HA)} \quad (22)$$

where the subscript i indicates position and the subscript j represents the present time step. This formulation is implicit in time because all positional derivatives are expressed at the new time step $(j + 1)$ and are solved as a vector of concentrations at all positions i. Each equation contains other species concentrations in the reaction terms [see Eqs. (8)–(11)] which are expressed explicitly (at the present time step) in terms of known values. The finite difference equation for each component is expressed in matrix form and solved one at a time for all concentrations C_i at the new time step $j + 1$. Each component equation is of the form

$$G \times \vec{X} = P$$

with $\vec{X}$ the unknown vector, G a tridiagonal, diagonally dominant matrix of values, and P the product vector composed of known constants. The Thomas method for efficient

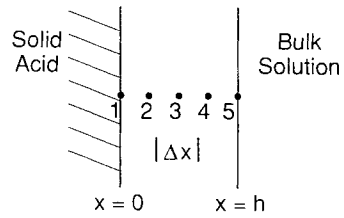

Fig. 4. Boundary layer with grid nodes.

sparse matrix decomposition was used to solve for $\vec{X}$ (22,23). Because significant round-off error is generated during the computation during matrix–vector multiplication, an iterative improvement routine was used after each such operation (23).

Convergence Criteria

At each time step, the matrix equations for each component were solved sequentially. The program checked the resultant concentration profile, C_i, for negative values, for intermediate maxima or minima, and for discontinuities. If these constraints of smoothness were satisfied, the change in value at each space point was evaluated between time steps to determine the closeness of approach to steady state. When the change between time steps became less than a specified amount, the mass rate of acid flow into and out of the control volume was calculated. Closure of the acid rate balance [Eq. (20)] over the control volume; i.e.,

$$\text{transport rate in} - \text{transport rate out} = \epsilon$$

indicated completion of the routine, where ϵ is a constant maximum allowable fraction of the average acid dissolution rate determined in the routine; generally 0.01. If this closure criterion was not met, the routine was continued, completing the specified maximum number of time steps. Both incoming and outgoing acid flux values were reported.

The performance of the routine for any set of experimental conditions was most dependent on the size of the time step and the reaction rate constants. The equilibrium reactions are extremely fast, so the forward and reverse rate constants are large ($\approx 10^7$ cm^3 μmol^{-1} sec^{-1}). Because the computation diverged when the program was run with actual rate constant values, it was necessary to use values several orders of magnitude smaller than the actual constants. Thus, the resulting concentration profiles did not represent equilibrium values. However, the dissolution rate calculated from those profiles was insensitive to the values of the rate constants as they were raised toward the maximum usable values for each system. The simulated acid flux reached a constant value asymptotically as the rate constants were raised. This behavior was noted for all three acids studied and is shown in Table II, where the reverse rate constants k_{r1} and k_{r2} are raised as the dimensionless time step (t_{val}) is set at a constant value. Further detail of the varied rate constant (VRC) model performance is given in the Appendix.

Elimination of Boundary Layer Constraint

The concentration boundary layer represents the area where "the major change in concentration occurs" (17). Because one goal of this study was to create a model free of adjustable parameters, the effect of imposing a defined, finite boundary layer thickness on the model results was tested. Because sink conditions (zero acid concentration) exist relatively far from the solid surface in the experimental system, the calculation of acid dissolution rate should be most accurate when a boundary layer is used which extends an infinite distance away from the dissolution face. That is, a complete model will not rely on a "correct" estimate of the boundary layer thickness. To test this hypothesis, boundary layers of double and triple the calculated distance, h, were used in the VRC model for a number of cases, and the dissolution rates calculated.

Table II. Calculated Acid Flux as a Function of Imposed Rate Constant (100 grid spaces, ω = 450 rpm)

Acid/solution pH	t_{val}	k_{r1}/k_{r2}	Flux × 10^8 (mol-cm^{-2} sec^{-1})
Benzoic/11	30	0/0	12.67
	30	100/400	12.59
	30	1000/4000	12.56
β-Naphthoic/10.5	65	0/0	0.551
	65	100/400	0.548
	65	200/800	0.547
	65	400/1600	0.545
	65	800/3200	0.543
β-Naphthoic/5	50	0/0	0.1274
	50	500/2000	0.1263
	50	1000/4000	0.1262
	50	2000/8000	0.1262
	50	4000/16000	0.1262
	50	6000/24000	0.1262
Indomethacin/6	65	0/0	1.058×10^{-2}
	65	1000/4000	1.055×10^{-2}
	65	2000/8000	1.055×10^{-2}
	65	4000/16000	1.055×10^{-2}
	65	8000/32000	1.054×10^{-2}
	65	12000/48000	1.054×10^{-2}
Indomethacin/9	50	0/0	2.195×10^{-2}
	50	1000/4000	2.191×10^{-2}
	50	2000/8000	2.192×10^{-2}
	50	4000/16000	2.194×10^{-2}
	50	8000/32000	2.195×10^{-2}
	50	12000/48000	2.196×10^{-2}

RESULTS AND DISCUSSION

Effect of Boundary Layer Thickness

The dissolution rate results for the VRC simulations using boundary layers of $1h$, $2h$, and $3h$ thickness (named VARYK, VARYK2, and VARYK3, respectively) are shown in Table III. There is a small but significant change (8–11%) in calculated fluxes when the boundary layer thickness is doubled in the numerical model, but less difference between the doubled and the tripled cases (0–6%). These differences are consistent with the work of Gregory and Riddiford (24), whose more complex expression gives a boundary layer thickness 3 to 5% larger than the Levich equation (12). The corresponding component profiles are shown in Figs. 5–7. Because the acid flux is determined from the HA and A^- concentrations [Eq. (21)], those profiles in which little difference is seen in panels a and b with different h reflect similar flux values as well. The benzoic acid case (Fig. 5) shows the most significant differences between the $1h$ and the $2h$ cases, with the $3h$ and $2h$ cases essentially identical. This result is reflected in Table III. Note that the VRC model results approach constant values asymptotically as the boundary layer size is increased. Because little change in calculated flux and the concentration profiles is shown using boundary layers $2h$ or $3h$ wide, the solution using $3h$ can be

Table III. Calculated Acid Flux: Limiting Effect of Boundary Layer Thickness on VRC Model Predictions

Acid	pH_b	Acid flux × 10^8 (mol-cm^{-2} sec^{-1}) Experimental data (7)	Predicted (VARYK)	Predicted (VARYK2)	Predicted (VARYK3)
Benzoic	7	9.60	11.57	10.32	10.25
β-Naphthoic	9	0.1499	0.1446	0.1326	0.1335
Indomethacin	9	3.382×10^{-2}	2.677×10^{-2}	2.391×10^{-2}	2.405×10^{-2}

considered a reasonable approximation to a solution with an infinite boundary layer thickness.

The results of all numerical simulations are presented in Table IV, showing that the calculated flux is reduced significantly when the boundary layer thickness is tripled. Identical time step size and rate constants were used for each acid/bulk pH simulation. Since the thickness modeled by VARYK3 was three times that used in VARYK, 300 grid spaces were used in VARYK3 to keep the space step size the same for both models. Alteration of the size of the model region has the greatest effect on benzoic acid, where calculated fluxes were 11–18% lower when the boundary layer thickness was tripled. The calculated flux was 7–15% lower for naphthoic acid and indomethacin.

Comparison of Present Model Results with Experimental Results and Previous Models

As shown in Table IV, the results of the dissolution

Table IV. Comparison of Acid Flux Predictions and Experimental Results (25°C, I = 0.5)

Acid	pH_b	Acid flux × 10^8 (mol-cm^{-2} sec^{-1}) J_{exp}[a]	J_{VARYK3}[b]	J_{VARYK}[b]	J_{diff}[a,b]
Benzoic	7	9.60[c]	10.25	11.57	9.24
	8	9.16	10.25	11.57	9.24
	9	9.91	10.26	11.58	9.25
	10	9.50	10.32	11.66	9.32
	11	10.73	10.88	12.56	10.11
	11.2	11.14	11.26	13.21	10.70
	11.4	12.17	11.96	14.31	11.70
	11.7	14.58	14.32	17.58	14.66
	12	23.23	20.22	24.76	20.96
	12.3	33.53	32.94	39.82	33.88
	12.61	64.38	59.93	71.62	61.11
	13.04	136.31[c]	150.1	178.5	151.7
β-Naphthoic	5	0.1185	0.1172	0.1262	0.0741
	6	0.1330	0.1248	0.1354	0.0817
	7	0.1382	0.1257	0.1364	0.0826
	8	0.1359	0.1265	0.1372	0.0834
	8.5	0.1417	0.1282	0.1391	0.0852
	9	0.1499	0.1335	0.1446	0.0908
	9.2	0.1615	0.1380	0.1498	0.0958
	9.5	0.1824	0.1505	0.1642	0.1101
	10.05	0.2736	0.2230	0.2542	0.1978
	10.2	0.3462	0.2717	0.3143	0.2538
	10.5	0.5622	0.4585	0.5394	0.4541
	10.7	—	0.6916	0.8160	0.6943
	11.0	—	1.336	1.576	1.348
Indomethacin	6	1.336×10^{-2}	1.286×10^{-2}	1.381×10^{-2}	0.77×10^{-2}
	7	1.506×10^{-2}	1.388×10^{-2}	1.499×10^{-2}	0.87×10^{-2}
	8	1.814×10^{-2}	1.482×10^{-2}	1.598×10^{-2}	0.96×10^{-2}
	8.5	2.272×10^{-2}	1.689×10^{-2}	1.826×10^{-2}	1.17×10^{-2}
	8.7	2.532×10^{-2}	1.872×10^{-2}	2.038×10^{-2}	1.37×10^{-2}
	9	3.382×10^{-2}	2.405×10^{-2}	2.677×10^{-2}	1.97×10^{-2}
	9.2	—	3.102×10^{-2}	3.525×10^{-2}	2.39×10^{-2}
	9.5	—	5.214×10^{-2}	6.061×10^{-2}	4.36×10^{-2}

[a] From Ref. 7.

[b] Used $D_H = 9.31 \times 10^{-5}$ cm^2 sec^{-1} and $D_{OH} = 5.28 \times 10^{-5}$ cm^2 sec^{-1} as documented by Cussler (28).

[c] Mean taken from at least two determinations.

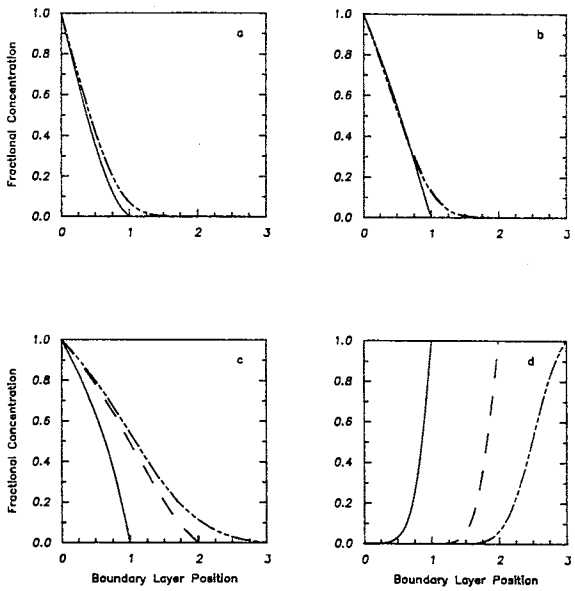

Fig. 5. Concentration profiles for benzoic acid, solution pH 7: effect of varied boundary layer thickness. (a) [HA]; (b) [A^-]; (c) [H^+]; (d) [OH^-]. ——, model run at 1h (VARYK); – –, model at 2h (VARYK2); —— – –, model at 3h (VARYK3).

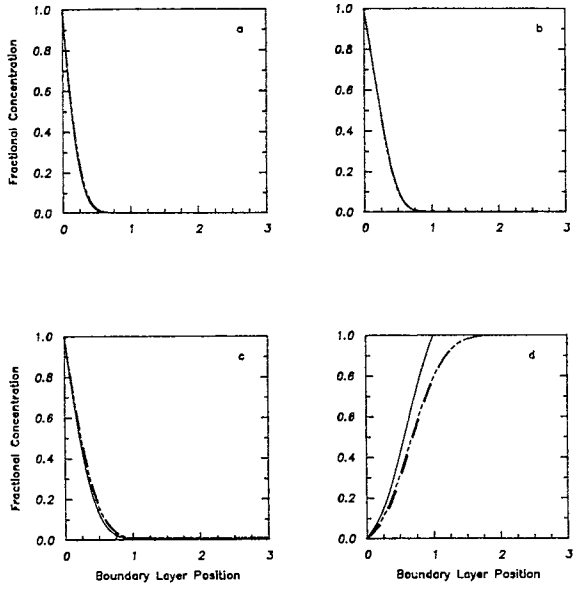

Fig. 7. Concentration profiles for indomethacin, solution pH 9: effect of varied boundary layer thickness. (a) [HA]; (b) [A^-]; (c) [H^+]; (d) [OH^-]. ——, model run at 1h (VARYK); – –, model at 2h (VARYK2); —— – –, model at 3h (VARYK3).

rates predicted by the VRC routine (J_{VARYK3}) are compared with experimental values (7), shown as J_{exp}, and with an earlier analytical solution which omitted the convective term, shown as J_{diff} (7). These predicted fluxes also are shown graphically in Figs. 8–10. The model deviates from the experimental data an average of 5.3% for benzoic acid, 10.5% for naphthoic acid, and 18.4% for indomethacin. Comparable figures for the earlier model show 5.7, 39.0, and 43.4% deviation, respectively, from the experimental results. It is evident that the present VRC model results are much closer to experimental flux data for most of the cases—due to the inclusion of convection.

The effect of convection is seen most clearly by comparing the component concentration profiles generated by the VRC numerical model with corresponding profiles from the diffusion/reaction model (7). Figure 11 shows concentration profiles for all three acids at solution pH 9. This figure illustrates two major convective effects in every case. First, the components whose concentrations decrease with increasing distance from the acid wall (HA, A^-, and H^+) decrease more rapidly than they would without convection. Second, the hydroxide ion concentration increases closer to the acid wall and has a less dramatic increase toward the outside of the boundary layer. Thus, the bulk flow toward the disk generated by its rotation appears to facilitate OH^-

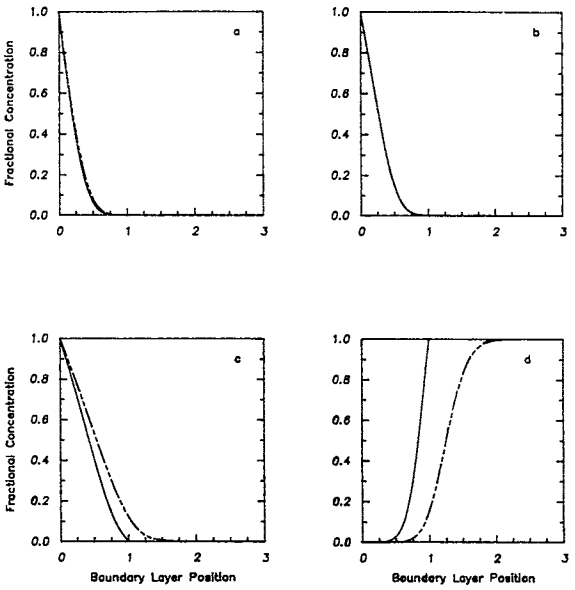

Fig. 6. Concentration profiles for β-naphthoic acid, solution pH 9: effect of varied boundary layer thickness. (a) [HA]; (b) [A^-]; (c) [H^+]; (d) [OH^-]. ——, model run at 1h (VARYK); – –, model at 2h (VARYK2); —— – –, model at 3h (VARYK3).

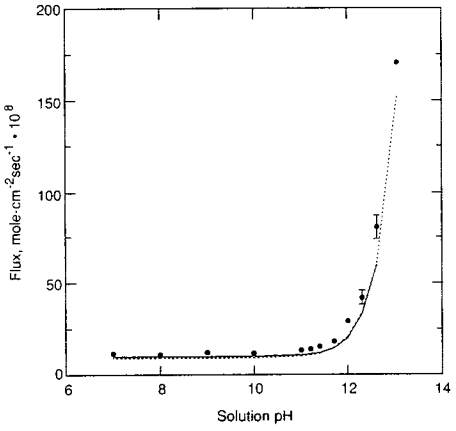

Fig. 8. Benzoic acid flux as a function of solution pH. *, experimental data (7); ——, prediction from VARYK3; - - -, prediction from diffusion-reaction model. Error bars show standard deviation of data (7).

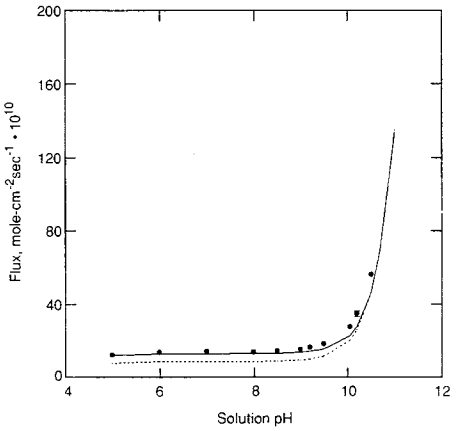

Fig. 9. β-Naphthoic acid flux as a function of solution pH. *, experimental data (7); ——, prediction from VARYK3; - - -, prediction from diffusion-reaction model. Error bars show standard deviation of data (7).

transport into the boundary layer and increased HA dissociation, as well as increased transport away from the disk.

Although the acid flux calculated using a $3h$ thickness (J_{VARYK3}) is lower than the result using $1h$ (J_{VARYK}), the agreement of the VRC model results with experimental results is consistently superior to the results obtained using the diffusion-reaction model (7), shown in Table IV as J_{diff}. That model uses the defined boundary layer thickness, h, as a key parameter which directly affects the model results. If the boundary layer thickness in the diffusion-reaction model were tripled, very poor results (mass fluxes one-third of those calculated) would result. Thus, the present VRC model can accurately calculate acid fluxes using an arbitrarily large boundary thickness. Note that there are no adjustable parameters save the limitation on the reverse rate constants, imposed by numerical necessity. Therefore, this model can be said to be predictive in that only first principles and independently measured parameters are used. The VRC model is superior to the diffusion-only model not only because its results are closer to experimental data, but also because it uses all physicochemical phenomena (convection, diffusion, reversible reaction) without arbitrarily set boundaries.

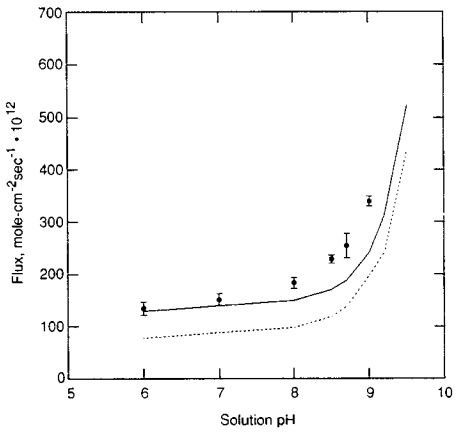

Fig. 10. Indomethacin flux as a function of solution pH. *, experimental data (7); ——, prediction from VARYK3; - - -, prediction from diffusion-reaction model. Error bars show standard deviation of data (7).

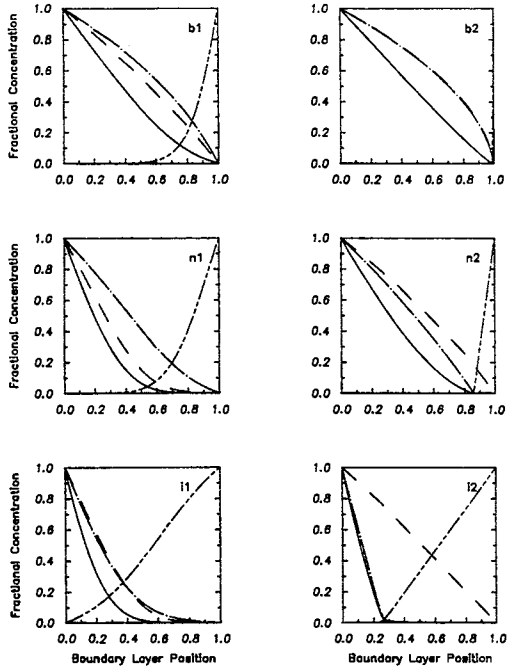

Fig. 11. Concentration profiles for dissolution of benzoic acid (panels b), β-naphthoic acid (panels n), and indomethacin (panels i) at pH_b 9. Panels numbered 1 are from the varied rate constant model; those numbered 2 are from the diffusion-reaction model (7). ——, [HA]; – –, [A^-]; — • — •, [H^+]; —— – –, [OH^-].

A comparison of the VRC model with the reaction plane (RP) model of McNamara and Amidon also is useful (14,25). Because the RP model uses the Levich-defined boundary layer thickness implicitly to calculate acid flux (14), it was compared with the VRC model using the same defined region, VARYK1. Table V shows the RP model result and the accompanying dissolution data tabulated with present VRC model results (generated using the physical properties of the reduced ionic strength solution used in that study). Results for the two acids studied, β-naphthoic acid and naproxen, are shown in the two sections of Table V. The VRC model predicts the experimental results of McNamara and Amidon (14) within an average of 10% for β-naphthoic acid and within an average of 11% for naproxen. The RP model predicts the same data within 14 and 8%, respectively. Thus, the current model is an improvement over the RP model for β-naphthoic acid but is not as close for naproxen. The inclusion of the acid–base reactions at all points in the boundary layer by the present method appears to simulate the experimental results as well as the reaction plane approach.

Both of these models include convective and diffusive transport. However, the RP model confines all chemical reactions to a single, defined plane, an adjustable parameter necessary for the computation of acid flux rates. Although the RP model simulates the experimental dissolution data as well as the VRC model, that approach does not reflect all phenomena occurring in acid dissolution; thus concentration profiles cannot be generated. The current VRC model does have this capability and includes all rate processes throughout a dissolution region free of artificial boundaries.

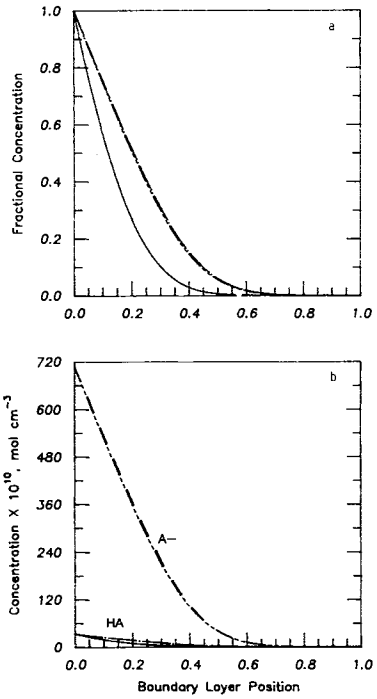

Fig. 12. Acid concentration profile for indomethacin, pH_b 9, shows effect of varied rate constant. ——, [HA] predicted with k_{r1}/k_{r2} = 12,000/48,000; —— •, [HA] predicted with k_{r1}/k_{r2} = 0/0; – –, [A^-] predicted with K_{r1}/k_{r2} = 12,000/48,000; —— – –, [A^-] predicted with k_{r1}/k_{r2} = 0/0. (a) Fractional concentration; (b) actual concentration.

Although the numerical model presented here represents a more accurate simulation of weak acid dissolution than earlier models, there remains some systematic discrepancy between the experimental data and the calculated flux values. The fractional error of the VRC model is greater when used with less soluble acids. That is, the indomethacin simulations had a greater fractional error from the data (an average of 18.4%) than the β-naphthoic acid simulations (10.5%) or the benzoic acid simulations (5.3%). Further, the errors for the highest pH_{bulk} conditions are relatively high, from 7 to 29%. It is unclear whether (a) some error inherent in the model fails to predict the transport mode at high solution pH, (b) experimental errors exist, or (c) an error in one or more chemical properties (solubility, diffusivity) causes the model-experimental difference. The deviation between the benzoic acid data and the VRC model may be attributable to inaccuracy in data collection (26); this acid was so soluble that the sampling and data recording systems may not have captured the rapidly changing concentration.

Limitations of the Model

As the pH of the bulk solution is decreased for a given dissolving acid, the interfacial pH approaches the bulk pH, and the dissolution rate is limited by the solubility of the undissociated acid. The VRC model calculates component concentrations through the boundary region only if a concentration gradient exists for all species. Thus, the model could not be used to simulate the dissolution of benzoic acid below pH 4, naphthoic acid below pH 5, or indomethacin below pH 6.

Table V. Comparison of Acid Flux Predictions with Reaction Plane Model (14,25) and Associated Experimental Results (14) (25°C, I = 0.1)[a]

Acid	pH_b	Acid flux × 10^{10} (mol-cm^{-2} sec^{-1}) J_{exp}	J_{VARYK}	J_{RP}
β-Naphthoic	2	7.50	—	7.50[b]
	4	11.9	—	10.73
	6	18.3	16.68	16.13
	7	—	16.79	—
	8	19.1	16.87	16.28
	8.5	—	17.05	—
	9	—	17.61	—
	9.5	—	19.54	—
	10	26.4	26.90	25.4
	10.05	—	28.44	—
	10.2	—	34.41	—
	10.5	—	56.86	—
	10.7	—	84.51	—
	11.0	—	160.5	—
	11.5	—	493.1	—
	11.72	969.0	814.0	734.0
Naproxen	2	3.30	—	3.30[b]
	4	3.80	—	4.16
	6	7.35	7.63	7.46
	7	—	7.74	—
	8	7.94	7.82	7.59
	9	—	8.58	—
	10	14.8	19.44	17.55
	10.5	—	51.63	—
	11.0	—	156.6	—
	11.2	—	246.6	—
	11.5	—	489.3	—
	11.72	763.0	810.3	724.7

[a] All values at 450-rpm disk rotation rate.
[b] Experimental value used as reference point for higher pH simulations; not determined by model.

Because the actual rapid reaction rates could not be used in the model, the concentrations of all components transported to and from the dissolving surface are not consistent with the equilibrium constants relating each component to any other. The magnitude of this inconsistency varies across the boundary layer and is confined to the H^+ and OH^- concentrations. As Fig. 12 illustrates, the absolute values of HA and A^- at any point are almost unchanged as the rate constant is altered. Thus the acid dissolution rate cal-

Table VI. Comparison of Benzoic Acid Flux Calculated Using Two Methods: Simulation at ω = 450 rpm, 25°C, I = 0.5

Solution pH	Acid flux × 10^8 (mol-cm^{-2} sec^{-1}) VRC model	Implicit model
7	11.57	11.74
8	11.57	11.74
9	11.58	11.75
10	11.66	11.80

Table VII. Effect of Time Step Size on Maximum Operable Rate Constant Ratio—Benzoic Acid, 100 Grid Spaces

Bulk solution pH	Dimensionless time step (t_{val})	k_1/k_2
7	250	400/1600
7	50	1000/4000
12	20	100/400
12	2	1000/4000

culated from the acid species concentrations is insensitive to the rate constant values. The inaccuracy generated by the reduced rate constants is seen only in the H^+ and OH^- concentration profiles and not in the acid flux calculation.

Validity of the Model Solution

The validity of the VRC solution was established by (a) comparing it to experimental results and (b) comparing it to the results of another solution method which requires equilibrium relationships at all points. The alternate solution method incorporated both convection and diffusion throughout the region modeled but was not numerically stable (22) for most of the acid-pH cases tested. This fully implicit method used a technique employed by Higuchi *et al.* (6) and later by Mooney *et al.* (7) where the differential equations for each of the interacting components were combined to eliminate the reaction terms. Two such combined differential equations were formed, and the acid and water equilibria formed the other two equations.

The implicit solution technique was analyzed for the source of the instability seen in most acid-pH cases. It was determined that the nonlinear equilibrium relationships, not convection, generated oscillatory behavior in computation (22). Although that method yields a solution only for a few cases, those results represent the complete solution of the steady state boundary value formulation using equilibrium reactions at every point. A comparison of results from the two methods will then indicate whether the VRC model solution is sufficiently close to the equilibrium condition to be used to accurately calculate acid dissolution rates. Table VI shows the flux of benzoic acid resulting from the two models using the Levich-defined boundary layer thickness. It is evident that the dissolution rates predicted by the two models are extremely close, the result of the equilibrium model lying within the range of the VRC result. Therefore, the VRC model is an accurate representation not only because it closely calculates experimental results, but also because its predicted values are the same as those generated by an exact solution to the transport equations when equilibrium at every point is used.

Mechanisms of Transport from the Rotating Disk

Although convection frequently has been omitted as a primary model of transport in dissolution modeling (7,15,16), it can be an important contributor to the overall dissolution rate. When dissolution from the rotating disk is simulated, convective effects should not be left out. Levich showed that (a) major concentration gradients are in the direction normal to the surface of the disk and (b) because the fluid motion in the radial and axial directions approaches zero at the rotating surface, dissolved acid enters from the rotating surface by diffusion only (17). Diffusion and disk-produced convection act together to move dissolved acid out of the boundary layer. Utilizing these facts, we have further found that the major mass transport away from the disk surface occurs in the direction *parallel* to the disk. This is shown using the acid flux equation (21), where the outgoing steady-state flux is split into the radial portion (out the sides of the cylindrical control volume) and the axial portion (out the flat outer surface at $x = h$). The results of this calculation show that, because the combined effects of fluid motion and diffusion within the boundary layer are large, negligible acid flux (less than 0.4% of the total) is transported across the outer boundary layer surface (at $x = 3h$); it is all moved radially. Only when the boundary layer is shortened to the Levich-defined thickness, h, with the more soluble benzoic acid, does a significant fraction of acid (30%) diffuse out the boundary layer parallel to the disk. Further, the incremental difference between the flux predictions of the earlier diffusion-reaction model (J_{diff}) and those of the present model (J_{VARYK3}) is the effect of convection. A comparison of these two predictions in Table IV shows that as much as 40% of the total flux can be attributed to convection.

CONCLUSION

The complete reaction-diffusion-convection model for transport of ionizable species from the rotating disk has been solved. This model provides a valid and accurate solution to the problem of weak acid dissolution and transport from the rotating disk. The model solution calculates acid dissolution

Table VIII. pH and Apparent Equilibrium Constant Values at Selected Points in a 100-Grid Space Boundary Layer—Indomethacin, $pH_{bulk} = 9$, $\omega = 450$ rpm

Space point No.	Apparent $K_a \times 10^2$ using k_{r1}/k_{r2} =			Apparent $K_w \times 10^7$ using k_{r1}/k_{r2} =			pH using k_{r1}/k_{r2} =		
	0/0	4K/16K	12K/48K	0/0	4K/16K	12K/48K	0/0	4K/16K	12K/48K
1	6.7	6.7	6.7	0.1	0.1	0.1	5.61	5.61	5.61
20	5.23	6.53	6.61	43.6	22.7	0.14	5.71	5.81	5.89
40	3.69	6.35	6.49	64.0	26.7	14.0	5.85	6.11	6.32
60	2.25	6.06	6.30	59.6	18.5	6.7	6.05	6.49	6.90
80	1.01	5.51	6.03	35.7	8.3	1.9	6.38	6.99	7.63
100	0.04	0.89	2.70	1.9	0.5	0.2	7.73	8.34	8.80

rates that are superior to earlier models, generally predicting acid flux within 10% of the observed values. Calculations of flux for the less soluble acids are closest to the experimental data in the physiological pH range, but there tends to be an underprediction at higher solution pH conditions.

Use of the classical definition of a concentration boundary layer thickness (17) adjacent to the rotating disk, an adjustable parameter required in earlier models, has been eliminated in this work. A more accurate solution of the model was determined for this study using a model region at least twice that defined in the literature. The experimental data of McNamara and Amidon (14) are predicted as closely using the VRC model as with a reaction plane model.

Finally, the present study has confirmed that convection in the radial direction is a significant mode of transport from the rotating disk. Acid diffuses from the solid–liquid interface and is moved away radially by the combined action of convective fluid motion and diffusion. The effect of convection is seen from a comparison of model-predicted concentration profiles of the four components in the experimental system with other model results which omit the convective term.

APPENDIX

Numerical Performance of the Solution Algorithm

As indicated above, several factors affected the ability of the computer program to be used to solve the acid transport equations. The values of the time step size, Δt, and the reverse rate constants, k_{r1} and k_{r2}, were the major determinants of whether the program would run to generate a valid solution. If the time step or any of the reaction rate constants was set at too great a value, the concentration profiles, C_i, generated by the computation contained negative values or were not smooth and constantly decreasing. Although the experimentally determined rate constants for benzoic acid and water reaction are known (27),

$$k_{r1} = 3.5 \times 10^7 \text{ cm}^3 \text{ mol}^{-1} \text{ sec}^{-1} \quad (23)$$

$$k_{r2} = 1.4 \times 10^8 \text{ cm}^3 \text{ mol}^{-1} \text{ sec}^{-1} \quad (24)$$

the routine did not run successfully with these large values. If the program was run using these rate constants, the absolute values of the concentrations and acid flux grew with successive time steps, diverging until one of the values exceeded the maximum size allowable on the computer. Using lower rate constant values while maintaining the equilibrium ratio k_{r2}:k_{r1}, allowed smooth computation. Although the maximum useable rate constants are much lower than the experimentally determined values, the calculated flux changes asymptotically as larger k values are used. Therefore, the result using maximized rate constants is approaching the equilibrium solution. This analysis is shown in Table II. The dimensionless time step size, t_{val}, shown in Table II was used to set the time step with respect to a given grid spacing. It is defined as

$$\text{tval} = D_H \frac{\Delta t}{(\Delta x)^2}$$

Although a similar numerical problem was observed when the time step size used was too high, the calculation of acid flux also was insensitive to changes in tval. However, there was a relationship between Δt and the rate constant values. By decreasing the time step, the values of k_{r1} and k_{r2} could be raised to higher values, as illustrated in Table VII. This observation was used in setting the optimal numerical constants for each acid simulated; using the minimum feasible time step size and maximizing the k values for that Δt.

The greatest effect of the lower rate constant values imposed in the computation was on the concentration profiles of the components in the system. Figure 12 shows the net effects of various rate constants on HA and A^- concentrations for indomethacin at bulk solution pH 9. It is evident that there is little absolute difference in the concentrations of both forms between the two cases; therefore little difference in flux is seen.

The effects of reduced rate constant on component concentrations also are reflected in the change in pH throughout the boundary layer. Table VIII shows that the concentration curves change as the rate constants are increased, changing the apparent equilibrium constants through the boundary layer. For example, the apparent value of K_w, calculated at any point as

$$K_w = [H^+][OH^-]$$

deviates from its correct value of 10^{-8} (mol-cm^{-3})^2, reaching a maximum at about space point 40 in the results shown in Table VIII. Although that deviation continues to appear as the reaction rate constants are raised, its magnitude decreases. As maximum rate constant values are used, over three-quarters of the deviation from the correct K_w value is eliminated. The acid and water equilibria [Eqs. (4) and (5)] are imposed as boundary conditions at the wall (space point 1), but not at other points. Thus, the rate of the reversible reactions is reflected in the closeness to the correct equilibrium constant value at each point in the solution.

Because the acid flux result approaches a constant value as the rate constants are raised (see Table II), it is expected that this part of the model solution would not change if the rate constants could be elevated further to their actual values. Only the concentrations of the four transported components would reflect the approach to equilibrium reaction rates, their values moving closer to meeting the true equilibrium constants, Eqs. (4) and (5).

ACKNOWLEDGMENTS

This work was supported by Grant GM-33387 from the National Institutes of Health and by a fellowship from the AMOCO Foundation.

REFERENCES

1. C. V. King and S. S. Brodie. The rate of dissolution of benzoic acid in dilute aqueous alkali. *J. Am. Chem. Soc.* 59:1375–1379 (1937).
2. A. W. Hixson, and S. J. Baum. Mass transfer and chemical reaction in liquid-solid agitation. *J. Ind. Eng. Chem.* 36:528 (1944).
3. G. R. Carmichael and S.-C. Chang. A three-zone model for mass transfer accompanied by equilibrium and very fast second-order irreversible reactions. *Chem. Eng. Sci.* 35:2463 (1980).

4. A. Fick. *Ann. Phys.* 94:59–86 (1855).
5. W. Nernst. Theorie der Reaktionsgeschwindigkeit in heterogenen Systemen. *Z. Phys. Chem.* 47:52–55 (1904).
6. W. I. Higuchi, E. L. Parrott, D. E. Wurster, and T. Higuchi. Investigation of drug release from solids II. *J. Am. Pharm. Assoc. Sci. Ed.* 47:376–383 (1958).
7. K. G. Mooney, M. A. Mintun, K. J. Himmelstein, and V. J. Stella. Dissolution kinetics of carboxylic acids I: Effect of pH under unbuffered conditions. *J. Pharm. Sci.* 70:13–22 (1980).
8. K. G. Mooney, M. Rodriguez-Gaxiola, M. Mintun, K. J. Himmelstein, and V. J. Stella. Dissolution kinetics of phenylbutazone. *J. Pharm. Sci.* 70:1358–1365 (1981).
9. J. B. Hansen and O. Hafliger. Determination of the dissociation constant of a weak acid using a dissolution rate method. *J. Pharm. Sci.* 72:429–431 (1983).
10. A. T. M. Serajuddin and D. I. Jarowski. Effect of diffusion layer pH and solubility on the dissolution rate of pharmaceutical acids and their sodium salts II: Salicylic acid, theophylline, and benzoic acid. *J. Pharm. Sci.* 74:148–154 (1985).
11. M. Litt and G. Serad. Chemical reactions on a rotating disk. *Chem. Eng. Sci.* 19:867 (1964).
12. H. Grijeels, L. van Bloois, D. J. A. Crommelin, and C. J. de Blaey. Dissolution at porous interfaces II. A study of pore effects through rotating disc experiments. *Int. J. Pharm.* 14:299–311 (1983).
13. M. Nicklasson A. Brodin, and L.-O. Sundelof. On the determination of true dissolution rate parameters from rotating disc experiments. *Int. J. Pharm.* 15:87–95 (1983).
14. D. P. McNamara and G. L. Amidon. Dissolution of acidic and basic compounds from the rotating disk: Influence of convective diffusion and reaction. *J. Pharm. Sci.* 75:858–868 (1986).
15. K. G. Mooney, M. A. Mintun, K. J. Himmelstein, and V. J. Stella. Dissolution kinetics of carboxylic acids II: Effect of buffers. *J. Pharm. Sci.* 70:22–32 (1980).
16. J. G. Aunins, M. Z. Southard, R. A. Myers, K. J. Himmelstein, and V. J. Stella. Dissolution of carboxylic acids III: The effect of polyionizable buffers. *J. Pharm. Sci.* 74:1305–1315 (1985).
17. V. G. Levich. *Physiochemical Hydrodynamics,* Prentice-Hall, Englewood Cliffs, NJ, 1962.
18. J. H. Wood, J. E. Syarto, and H. Letterman. Improved holder for intrinsic dissolution rate studies. *J. Pharm. Sci.* 54:1068 (1965).
19. R. A. Robinson and R. H. Stokes. *Electrolyte Solutions,* Butterworths, London, 1959.
20. R. B. Bird, W. E. Stewart, and E. N. Lightfoot. *Transport Phenomena,* Wiley, New York, 1960.
21. M. Z. Southard. *Transport Mechanisms of Weak Acid Dissolution in Aqueous Solutions of Variable pH,* Ph.D. dissertation, University of Kansas, Lawrence, 1988.
22. B. Carnahan, H. A. Luther, and J. O. Wilkes. *Applied Numerical Methods,* Wiley, New York, 1969.
23. W. H. Press, B. P. Flannery, S. A. Teukolsky, and W. T. Vettering. *Numerical Recipes—The Art of Scientific Computing,* Cambridge University Press, New York, 1986.
24. D. P. Gregory and A. C. Riddiford. Transport to the surface of a rotating disc. *J. Chem. Soc.* 3756 (1956).
25. D. P. McNamara. Personal communication, Boehringer Ingelheim Corp. (1988).
26. V. J. Stella. Personal communication, University of Kansas, Lawrence (1988).
27. M. Eigen. Proton transfer, acid-base catalysis, and enzymatic hydrolysis. *Angew. Chem. Int. Ed.* 3:1–19 (1964).
28. E. L. Cussler. *Diffusion: Mass Transfer in Fluid Systems,* Cambridge University Press, New York, 1984.